



OPEN

Optimizing blended cement concrete strength using the Box-Behnken design technique

Solomon Oyeibisi^{1,2✉}, Mahaad Issa Shammass³, Mohammed Seyam¹ & Bonga Praisegod Khuzwayo¹

A properly optimized concrete mix design yields the required workability and strength for the fresh and hardened concrete to sustain desired loads and stresses over time, preventing premature failure. Thus, it is imperative to investigate the behavioural sensitivity of blended cement concrete to mix design variations. The research uses the Box-Behnken design of the response surface method to optimize the slump and compressive strength of blended cement concrete incorporating Shea nutshell ash (SNA). SNA was partially utilized as a Portland limestone cement (PLC) substitute at 5–15 wt% replacement levels using C25, C30, and C40 MPa mix design proportions and tested for compressive strength after 7–90 curing ages. Binder (SNA-to-PLC) ratio, water-to-binder ratio, binder-to-aggregate ratio, and curing age were engaged as continuous (independent) variables to optimize the response (dependent) variables (slump and compressive strength). The slump and compressive strength responses were optimized by the Box-Behnken design. The results exhibited a minimized slump and a maximized compressive strength with approximately 40–63% reduction and 10% increment. The correlations between the optimized and experimental variables were accurate and strong, with 98.89% and 98.44% R^2 for slump and compressive strength. Ultimately, this response model is beneficial in determining the optimum mix design proportions to achieve the desired compressive strength of blended cement concrete incorporating repurposed waste materials.

Keywords Blended cement concrete, Compressive strength, Modelling, Optimization, Recycling, Response surface methodology

Concrete is the most widely used building material in the world, and cement is an essential ingredient in its creation. However, considerable ecological harm is caused by high energy consumption and excessive CO_2 emissions during cement manufacture, accounting for 2–3% of global energy consumption and 5–8% of global emissions¹. Using waste materials as substitutes for cement promotes recycling and addresses environmental challenges from the excessive utilization of cement². Shea nutshell is the primary solid waste of agricultural products. According to the Food and Agriculture Organization of the United Nations, global production of sheanuts in 2023 was 870784.49 metric tons from a harvested area of 720,571 ha³. Recycling shea nutshell ash (SNA) as an alternative to Portland limestone cement (PLC) lowers blended cement concrete's embodied energy and global warming potential while simultaneously improving its sustainability score and eco-strength efficiency⁴. SNA calcined at 750 °C for 5 h resulted in a 3% reduction in embodied energy and a 5% reduction in global warming and global temperature potentials for every 5% substitution of SNA for PLC. In addition, the blended cement concrete was 2–5% and 1–2% more cost-effective and sustainable at 5–20% SNA replacement than Portland limestone cement concrete⁴. The physical characteristics, strength, and durability of blended cement concrete were improved by replacing cement and fine aggregates with 15 wt% kaolin clay and 30 wt% shea nutshell particles⁵.

Variables, such as mix proportions (cement, water, and aggregates), curing conditions, temperature, compaction, and concrete age, influence the fresh and hardened properties of concrete. Utilizing the conventional experimental design approach necessitates conducting numerous, costly, and time-consuming tests to assess the impact of various variables at different levels on concrete properties. However, given a limited number of experiments, a suitable Design of Experiment (DoE) can be utilized to assess the influence of these factors⁶. A crucial component of concrete technology is the quantity of concrete ingredients, which guarantees economy,

¹Civil Engineering and Geomatics Department, Durban University of Technology, Durban, South Africa. ²Civil Engineering Department, The University of the South Pacific, Suva, Fiji. ³Civil and Environmental Engineering Department, Dhofar University, Salalah, Sultanate of Oman. ✉email: solomonO@dut.ac.za

safety, and quality. The concrete mix proportions are achieved by applying particular guidelines and the suitable process to choose the optimum element compositions and satisfy the intended objectives or qualities. The ultimate goal is to maximize anticipated rewards while minimizing needed effort⁷. Consequently, an optimization that assesses the conditions of a function and minimizes or maximizes the values can be used to describe the necessary action or the intended application in any real-world situation⁷. The mix design optimization results in cost savings by reducing material consumption while maintaining the necessary performance⁸.

Design of Experiment (DoE) is a statistically based technique for examining process parameters and outcomes. DoE produces the most results, minimizes the experimental numbers, and shows a mathematical relationship between a response and factors⁹. Response surface method (RSM), a subset of DoE, has a number of uses in industrial process optimization¹⁰. RSM is a mathematical optimization technique that combines statistical analysis, design, and optimization, providing benefits in multi-parameter analysis¹¹. Contrary to the central composite design (CCD) of RSM, the Box-Behnken design (BBD) tests each variable at three levels: low, middle, and high (typically denoted by the codes -1 , 0 , and $+1$). In addition to a central point, BBD incorporates points at the midpoints of the boundaries of the design space, fitting a quadratic model with fewer experiments for optimizing than a full factorial design. BBD saves time and money by reducing the number of experiments required. BBD fits a second-order model, known as a quadratic model, which is helpful for comprehending how variables relate to the response. Because the designs are frequently rotatable, the variance of the forecasts is consistent between directions in the design space¹². Similarly, BBD permits all design points to be within the safe operating ranges while optimizing⁸.

From the literature perspective, a recent comprehensive review of cementitious mix optimization using RSM revealed that the two most popular methods are CCD and BBD, which provide distinct ways to investigate how variables and responses interact in the cementitious mix design compared to full factorial design (FFD)¹³. For instance, BBD of RSM was engaged to maximize the compressive strength of recycled aggregate-based concrete, considering waste concrete powder (WCP), water-to-cement ratio, recycled fine aggregate replacement ratio, and curing ages of 3, 28, and 90 days. The results showed that a suitable quantity of WCP is advantageous for enhancing the early-age and late-age compressive strengths with 15 wt% and 0.43 optimal dosages of the fine aggregate and water-to-cement ratio¹⁴. The BBD-based experimental investigation for maximizing the ratios of cementitious ingredients of activated lithium slag composite cement revealed that activated lithium slag composite cementitious materials exhibited optimum performance at 7.30 wt% activated lithium slag, 8.80 wt% sodium silicate content, and a water-to-solid ratio of 0.60:1¹⁵. In addition, the composite cementitious material under this ratio performed exceptionally well, with fluidity, gelation time, and water evolution rate of 235.69 mm, 73.54 s, and 1.123%, and compressive strengths of 11.54 and 22.90 MPa at 3 and 28 curing ages¹⁵. Optimizing cement paste backfill materials via BBD demonstrates optimal mix proportions at 76.75 wt% 3.35, 0.10, and 1.24% for mass concentration, tailing-to-rock ratio, cement-tailing ratio, and pumping agent, with slump and unconfined compressive strength having optimal mixtures of 24.10 cm and 1.59 MPa¹⁶. The BBD-based optimization of new eco-friendly building materials based on slag activated by diatomaceous earth demonstrated optimal proportions at the liquid-to-solid ratio, sodium hydroxide molarity, and diatomaceous earth content of 0.59, 7.50 mol l⁻¹, and 9.50 wt%, yielding enhanced compressive strength, bulk density, porosity, and water absorption of 42 MPa, 1.67 g cm⁻³, 18.98%, and 11.27%¹⁷. There is little to no research on using BBD to optimize the mix proportions of blended cement concrete incorporating SNA, despite the encouraging trend of studies on using BBD as an RSM tool to optimize the concrete mix proportions. This motivates the conduct of this research.

This study engages BBD to optimize the slump and compressive strength of blended cement concrete incorporating SNA. Shea nutshells were calcined at 750 °C for 5 h, obtaining SNA. Portland limestone cement (PLC) was replaced by 5–15 wt% SNA using C25, C30, and C40 MPa mix design proportions and tested for compressive strength after 7–90 curing ages. Binder ratio, water-to-binder ratio, binder-to-aggregate ratio, and curing age were used as continuous (independent) variables to optimize the response (dependent) variables (slump and compressive strength). The experimental and optimized values were compared and modeled. These findings would enhance the utilization efficiency of binders (PLC and SNA) and the functionality and application scenarios of blended cement concrete.

Materials and methods

Materials

All materials used, such as 42.5R PLC, shea nutshells, fine aggregates (FA, ≤ 4.75 mm particle sizes), and coarse aggregates (CA, ≤ 12.50 mm particle sizes), were locally sourced. Shea nutshells were calcined at 750 °C for 5 h, obtaining about 25 wt% SNA, and sieved to BS 45- μ m size. Heating, or calcination, at particular temperatures influence the pozzolanic reactivity of supplementary cementitious materials (SCMs). Although reactivity tends to increase with temperature, there is an ideal range where the maximal reactivity is attained. Nevertheless, overheating may cause reactivity to decline¹⁸. The oxide compositions of PLC and SNA, as shown in Fig. 1, were analyzed using the XRF spectrophotometer machine, Philips PW-1800. The physical properties. The binding materials (PLC and SNA) were analyzed for fineness, specific gravity, and specific surface area following the BS EN¹⁹. Likewise, FA and CA were tested for specific gravity, moisture content, and water absorption following BS EN²⁰. Table 1 presents the physical properties of binding materials and aggregates. Figure 2a shows the particle size distribution (PSD) of the binding materials as determined by laser diffraction with a Beckman Coulter LS-100 model, while Fig. 2b displays the aggregate grades with lower limits (LL) and upper limits (UL)²⁰. According to the findings in Fig. 1, SNA met the pozzolanic requirements outlined in BS EN 450-1²¹ and BS EN 8615-2²², such that the addition of SiO₂ (62.15%), Al₂O₃ (18.78), and Fe₂O₃ (8.10%) satisfied the minimum requirement of 70%.

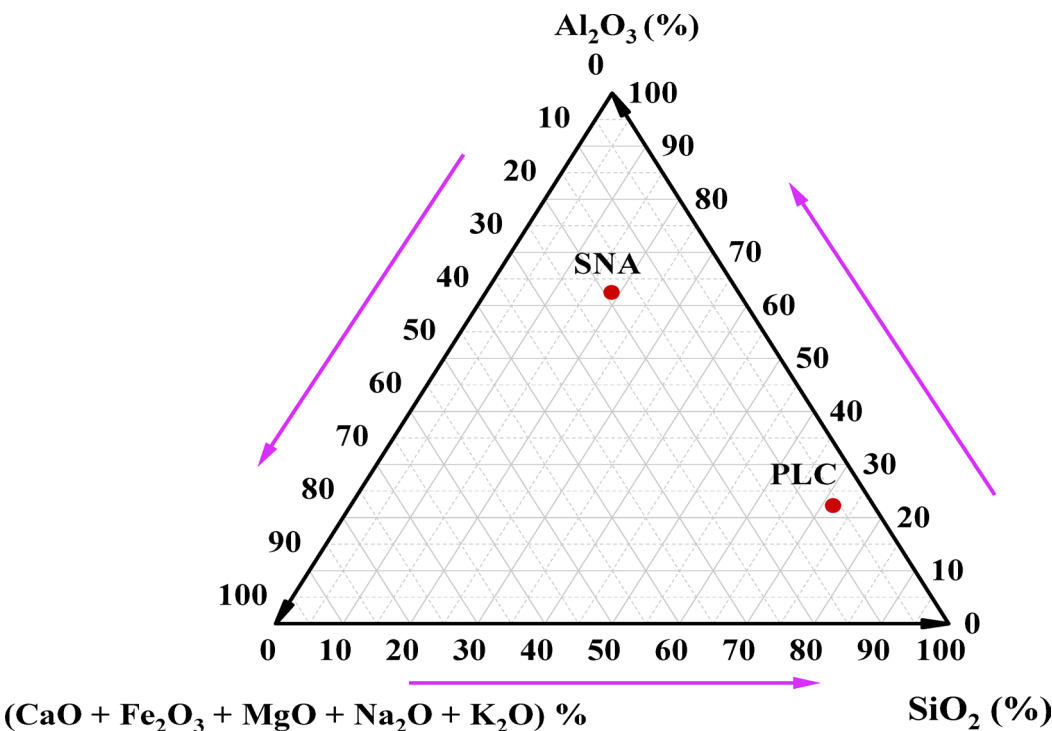


Fig. 1. Ternary diagram of oxide compositions of binding materials.

Physical	PLC	SNA	FA	CA
Specific gravity	3.15	2.45	2.60	2.69
Fineness (%)	7.63	7.80	–	–
SSA (m ² kg ^{−1}) Blaine	375	495	–	–
Water absorption (%)	–	–	0.30	0.20
Moisture content (%)	–	–	0.70	0.80

Table 1. Physical properties of materials used.

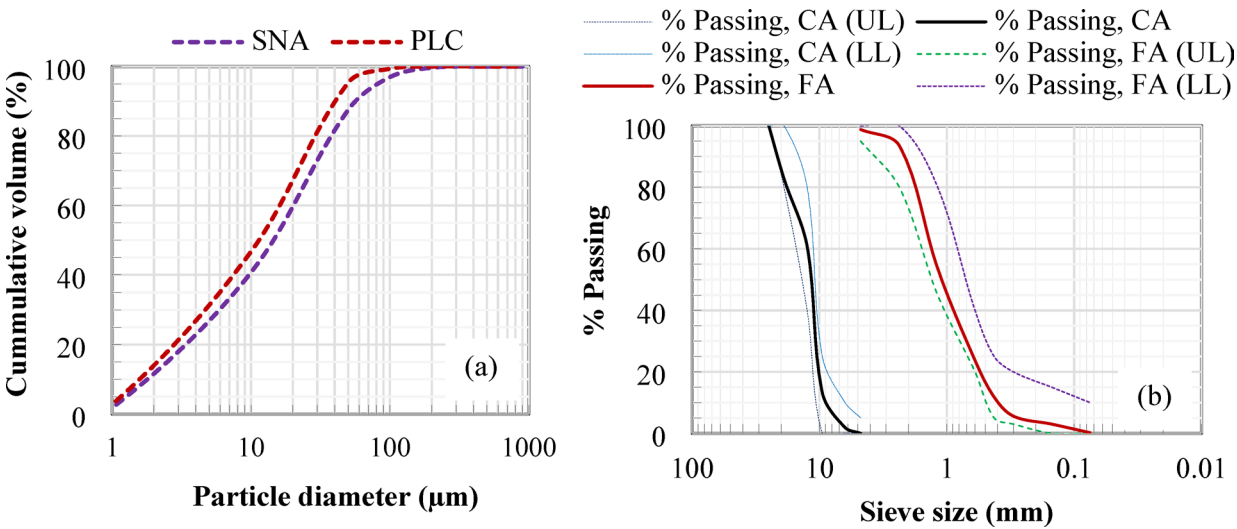


Fig. 2. Particle size distributions for (a) binding materials and (b) aggregates.

Grade	Mix ID	PLC	SNA	FA	CA	Water
C25 MPa	PA0 (100 PLC) wt%	340	0	715	1035	210.80
	PA5 (95 PLC + 5 SNA) wt%	323	17	715	1035	210.80
	PA10 (90 PLC + 10 SNA) wt%	306	34	715	1035	210.80
	PA15 (85 PLC + 15 SNA) wt%	289	51	715	1035	210.80
C30 MPa	PJ0 (100 PLC) wt%	390	0	675	1031	210.60
	PJ5 (95 PLC + 5 SNA) wt%	370	20	675	1031	210.60
	PJ10 (90 PLC + 10 SNA) wt%	350	40	675	1031	210.60
	PJ15 (85 PLC + 15 SNA) wt%	330	60	675	1031	210.60
C40 MPa	PN (100 PLC) wt%	500	0	585	1030	210
	PN5 (95 PLC + 5 SNA) wt%	475	25	585	1030	210
	PN10 (90 PLC + 10 SNA) wt%	450	50	585	1030	210
	PN15 (85 PLC + 15 SNA) wt%	425	75	585	1030	210

Table 2. Concrete mix design proportions (kg/m³).

S/N	Variables	Type	Goal	Notation (Name)	Coded values		
					Low −1	Central 0	High +1
1	Binder ratio [SNA/(SNA + PLC)]	Independent	Minimize	E	0.05	0.10	0.15
2	Water-to-binder ratio	Independent	Minimize	F	0.42	0.52	0.62
3	Binder-to-aggregate ratio	Independent	Minimize	G	0.19	0.25	0.31
4	Curing age (days)	Independent	Minimize	H	7	48.50	90
5	Slump (mm)	Dependent	Minimize	S	33	49	65
6	Compressive strength (MPa)	Dependent	Maximize	CS	18.45	34.97	51.48

Table 3. Variables at three various levels for BBD.

Experimental methods

Concrete mix design proportions

The concrete mix design proportions were created using the methodology outlined in BS EN 206²³. Relevant research showed that the replacement level for SNA in concrete production is optimal at 15 wt%, satisfying the design strengths for structural applications⁴. As a result, 5–15 wt% SNA was used to replace PLC for proportioning concrete mix having design strengths of C25, C30, and C40 MPa, as detailed in Table 2.

Sample preparation and experimental tests

The fresh concrete samples were prepared following the methodology outlined in BS EN 12390-2²⁴. Fresh blended concrete samples were evaluated for workability using the slump test. A typical cone with interior specifications of 200 mm base diameter, 300 mm height, and 100 mm top diameter in accordance with BS standards was employed for test²⁵. The compressive strengths were tested on 150 mm³ cubes²⁶. All concrete samples were cured by water immersion at 23 ± 5 °C and 65 ± 5% RH and tested after 7, 28, and 90 days. Each mix ID was made in triplicate, and the mean of each mix sample was used.

Design of experiment (DoE)

Box-Behnken design (BBD)

The Box-Behnken was used to design the proportions of PLC-SNA-based blended concrete using binder ratio, water-to-binder ratio, binder-to-aggregate ratio, and curing age were used as continuous (independent) variables, and slump and compressive strength as the response (dependent) variables. Four distinct independent variables, as shown in Table 3, were used to build the BBD using Minitab 18 statistical software. Hence, Eq. (1) was applied to determine the number of design points^{8,13}. Table 4 displays the programme parameters and experimental results.

$$\text{Number of design points} = 2i(i - 1) + k \quad (1)$$

where i connotes independent variables, and k represents central-point runs, which is 3 by default.

The number of design points based on three and four independent variables with three central-point runs for slump and compressive strength, as indicated in Table 3, was fifteen (15) and twenty-seven (27) runs following Eq. (1). A full quadratic polynomial, as shown in Eq. (2), produces a high precision by precisely optimizing the relationship between the independent and dependent variables^{8,12,13}.

Mix ID	Std order	Run order	Pt type	Block	E	F	G	H	Slump (mm)	Compressive strength (MPa)
PA5	1	1	2	1	0.05	0.62	0.19	7	65	18.45
PA5	2	2	2	1	0.05	0.62	0.19	28		28.94
PA5	3	3	2	1	0.05	0.62	0.19	90		32.63
PA10	4	4	2	1	0.10	0.62	0.19	7	57	18.72
PA10	5	5	2	1	0.10	0.62	0.19	28		29.32
PA10	6	6	2	1	0.10	0.62	0.19	90		32.97
PA15	7	7	2	1	0.15	0.62	0.19	7	50	19.05
PA15	8	8	2	1	0.15	0.62	0.19	28		30.07
PA15	9	9	2	1	0.15	0.62	0.19	90		33.1
PJ5	10	10	2	1	0.05	0.54	0.23	7	63	21.04
PJ5	11	11	2	1	0.05	0.54	0.23	28		35.29
PJ5	12	12	2	1	0.05	0.54	0.23	90		38.83
PJ10	13	13	2	1	0.10	0.54	0.23	7	50	21.43
PJ10	14	14	2	1	0.10	0.54	0.23	28		35.75
PJ10	15	15	2	1	0.10	0.54	0.23	90		39.05
PJ15	16	16	2	1	0.15	0.54	0.23	7	46	21.96
PJ15	17	17	2	1	0.15	0.54	0.23	28		35.95
PJ15	18	18	2	1	0.15	0.54	0.23	90		39.21
PN5	19	19	2	1	0.05	0.42	0.31	28	55	46.94
PN5	20	20	2	1	0.05	0.42	0.31	7		27.26
PN5	21	21	2	1	0.05	0.42	0.31	90		50.65
PN10	22	22	2	1	0.10	0.42	0.31	7	45	27.74
PN10	23	23	2	1	0.10	0.42	0.31	28		47.49
PN10	24	24	2	1	0.10	0.42	0.31	90		50.93
PN15	25	25	2	1	0.15	0.42	0.31	7	40	28.13
PN15	26	26	2	1	0.15	0.42	0.31	28		48.25
PN15	27	27	2	1	0.15	0.42	0.31	90		51.48

Table 4. Programme parameters and response surface design creation.

$$Y = a_0 + \sum_{i=1}^n a_i x_i + \sum_{i=1}^n a_{ii} x_i^2 + \sum_{i < j} a_{ij} x_i x_j$$

(2)

where Y = dependent variables (slump and compressive strength).

- a₀ = model coefficient constant
- x_i, x_j = independent variables (E, F, G, and H)
- a_i = linear coefficient
- a_{ii} = quadratic coefficient
- a_{ij} = interaction coefficient.

Optimization of variables

Following the optimization concept, independent variables (E, F, G, and H) were minimized, while the dependent variables, such as slump and compressive strength, were minimized and maximized. The concrete's slump was minimized using binder ratio, water-to-binder ratio, and binder-to-aggregate ratio, while the compressive strength was maximized with binder ratio, water-to-binder ratio, binder-to-aggregate ratio, and curing age. This is because curing age takes no part in determining concrete slump. Concrete slump is determined immediately after achieving a homogenous mixture. In accordance with this idea, the dependent variables' values were transformed into a composite desirability function (D) that spans between 0 and 1, as illustrated in Eq. (3)^{8,27}. The optimization is better when the composite desirability is around 1⁸.

$$0 \leq D \leq 1$$

(3)

Equation (3) states that if the response value is at its objective or goal, D = 1. Furthermore, D = 0 in the event that the value falls outside of an allowed range. In addition, to maximize, minimize, or make the response as close to the target as possible, the desirability is composite based on the expressions shown in Eqs. (4)–(6)^{6,27,28}. Figure 3 displays the flow diagram of the BBD optimization process for concrete mixes.

$$\begin{cases} D = 0 & \text{if } r \leq L \\ D = \left(r - \frac{L}{T} - L\right)^w & \text{if } L \leq r \leq T \\ D = 1 & \text{if } r \geq T \end{cases}$$

(4)

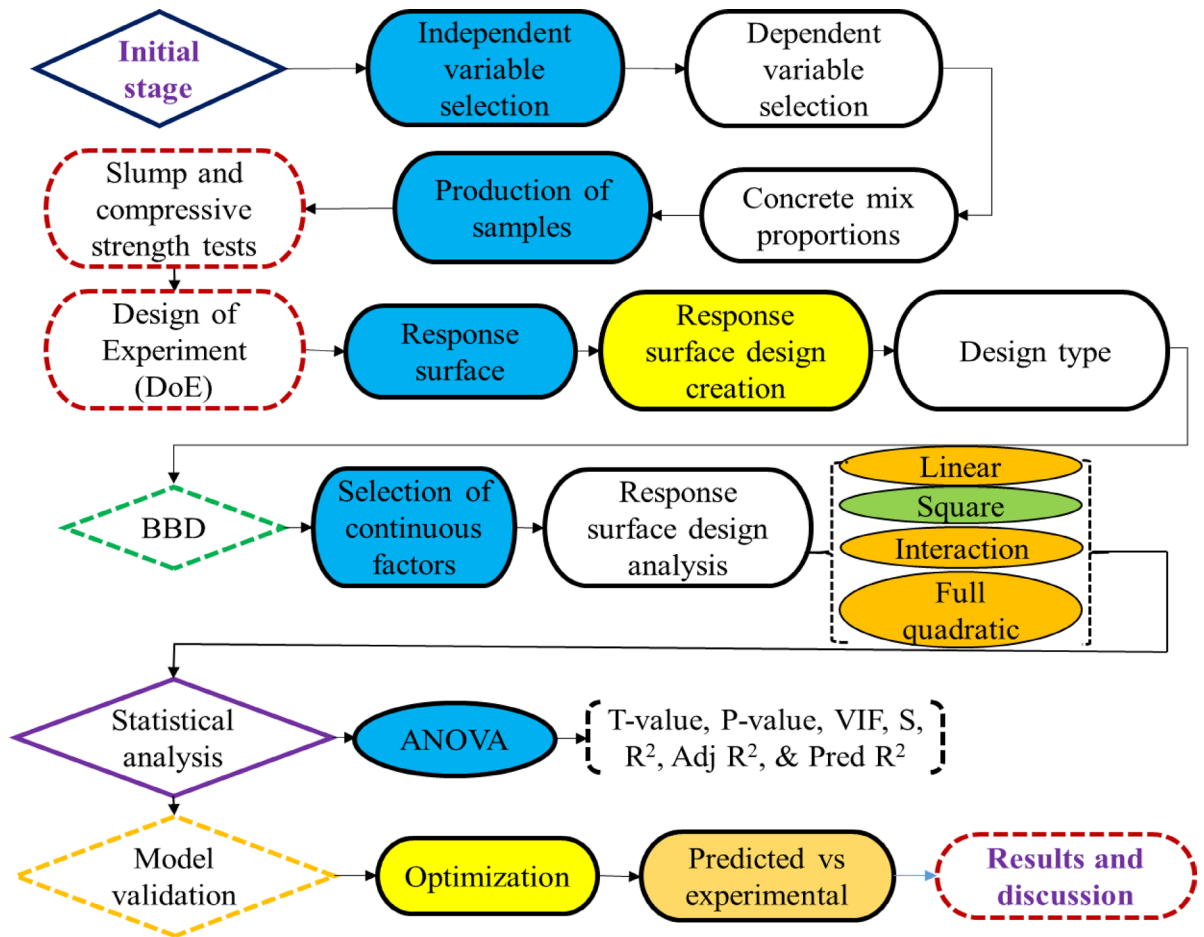


Fig. 3. Flow diagram of the BBD optimization process for concrete mixes.

$$\begin{cases} D = 1 & \text{if } r \leq T \\ D = \left(r - \frac{U}{T} - U\right)^w & \text{if } T \leq r \leq U \\ D = 0 & \text{if } r \geq U \end{cases} \quad (5)$$

$$\begin{cases} D = \left(r - \frac{L}{T} - L\right)^{w1} & \text{if } L \leq r \leq T \\ D = 1 & \text{if } r = T \\ D = \left(r - \frac{U}{T} - U\right)^{w2} & \text{if } T \leq r \leq U \\ D = 0 & \text{if } r = L \\ D = 0 & \text{if } r = U \end{cases} \quad (6)$$

where D represents the composite desirability function (0–1), r connotes the response, L , U , and T indicate lower, upper, and target values, and w refers to the weight.

Results and discussion

Response surface design analysis

The statistical responses, following the response surface design analysis, are presented in Figs. 4 and 5. The residuals, or the difference between the observed and the fitted response variables, are not considerably affected in practice by a balanced or nearly balanced design with a high number of observations if it deviates moderately from a straight line or normalcy⁸. Therefore, a balanced design necessitates regularly distributed residuals from the any study. The slump and compressive strength normal probability plots in Fig. 4a and b demonstrated that the data followed a normal distribution since the points fell in an approximately straight line along the fitted line. Likewise, the heights of the bars in Fig. 5a and b for the slump and compressive strength followed the shape of the lines, demonstrating that the dataset fit the distribution well.

The analysis of variance (ANOVA) and fitted coefficients results are presented in Tables 5 and 6 for slump and Tables 7 and 8 for compressive strength. The analysis of variance (ANOVA) was used to examine the effects of independent factors and the model's precision on the slump and compressive strength of blended cement concrete. The square models (water-to-binder ratio (F) and binder-to-aggregate ratio (G)) and a 2-way interaction model (water-to-binder ratio (F) and binder-to-aggregate ratio (G)) were removed from the analysis

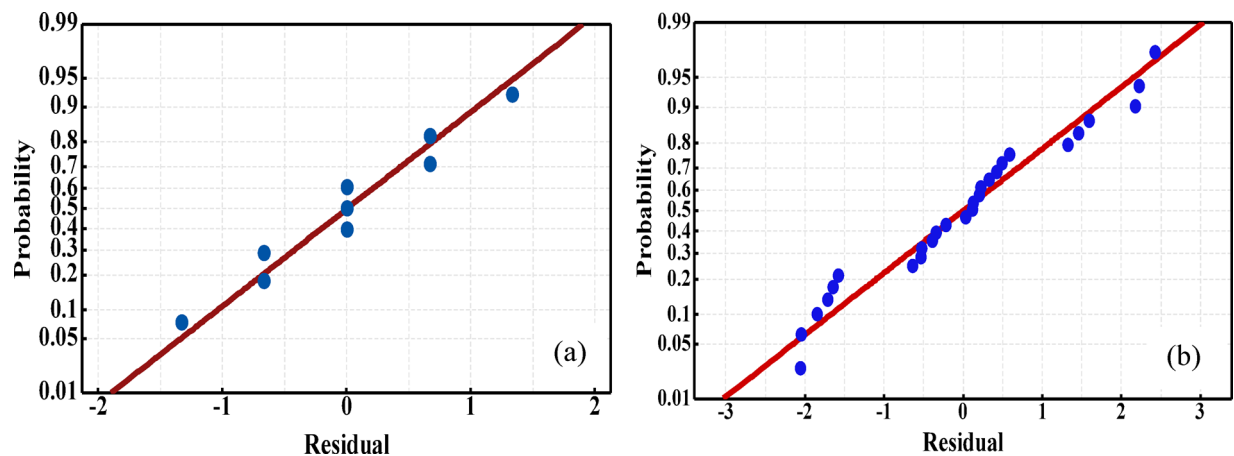


Fig. 4. Normal probability plots for (a) slump and (b) compressive strength.

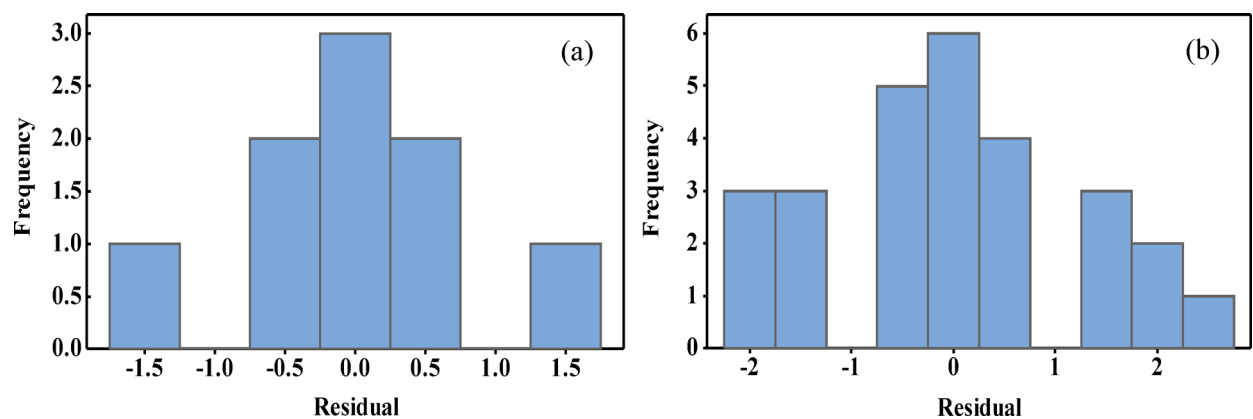


Fig. 5. Histogram plots for (a) slump and (b) compressive strength.

Source	DF	Adj SS	Adj MS	F-Value	P-Value
Model	6	554.667	92.444	34.67	0.028
Linear	3	397.667	132.556	49.71	0.020
E (Binder ratio)	1	225.000	225.000	84.37	0.012
F (Water-to-binder ratio)	1	1.167	1.167	0.44	0.576
G (Binder to-aggregate ratio)	1	0.009	0.009	0.00	0.959
Square	1	12.500	12.500	4.69	0.163
E ²	1	12.500	12.500	4.69	0.163
2-way interaction	2	1.333	0.667	0.25	0.800
E × F	1	1.286	1.286	0.48	0.559
E × G	1	1.316	1.316	0.49	0.555
Error	2	5.333	2.667		
Total	8	560.000			

Table 5. ANOVA for the slump.

due to their non-significant effects. Consequently, only the binder ratio demonstrated a significant linear effect on the slump of blended cement concrete because the P-value (0.012) was lower than the significance level (α -level, 0.05), while the F-value (84.37) was greater than 5^{6,8,29}. This result affirms the previous research, which demonstrated that the use of supplementary cementitious materials (silica fume, fly ash, and quartz powder) as binding materials, has a significant effect on the workability properties of the blended cement pastes³⁰. The variance inflation factor (VIF) shows the extent to which the correlations between the model's predictors inflate a coefficient's variance in a regression analysis. In general terms, variables are considered to be non-correlated,

Term	Coef	SE Coef	T-Value	P-Value	VIF
Constant	50.33	1.02	49.43	0.000	
E (Binder ratio)	- 7.500	0.816	- 9.19	0.012	1.50
F (Water-to-binder ratio)	5.83	8.82	0.66	0.576	177.33
G (Binder to-aggregate ratio)	0.50	8.72	0.06	0.959	177.33
E ²	2.50	1.15	2.17	0.163	1.00
E × F	7.5	10.8	0.69	0.559	178.50
E × G	7.5	10.7	0.70	0.555	180.50

Table 6. Fitted (coded) coefficients for the slump.

Source	DF	Adj SS	Adj MS	F-Value	P-Value
Model	11	2815.68	255.97	86.92	0.000
Linear	4	2142.66	535.66	181.89	0.000
E (Binder ratio)	1	2.07	2.07	0.70	0.415
F (Water-to-binder ratio)	1	0.00	0.00	0.00	0.972
G (Binder to-aggregate ratio)	1	5.91	5.91	2.01	0.177
H (Curing age, day)	1	1070.84	1070.84	363.62	0.000
Square	2	585.56	292.78	99.42	0.000
E ²	1	0.00	0.00	0.00	0.973
H ²	1	585.56	585.56	198.83	0.000
2-way interaction	5	41.68	8.34	2.83	0.054
E × F	1	0.03	0.03	0.01	0.924
E × G	1	0.03	0.03	0.01	0.915
E × H	1	0.09	0.09	0.03	0.866
F × H	1	0.06	0.06	0.02	0.890
G × H	1	0.06	0.06	0.02	0.890
Error	15	44.17	2.94		
Total	26	2859.86			

Table 7. ANOVA for the compressive strength.

Term	Coef	SE Coef	T-Value	P-Value	VIF
Constant	46.246	0.967	47.85	0.000	
E (Binder ratio)	0.421	0.502	0.84	0.415	1.54
F (Water-to-binder ratio)	-0.19	5.45	-0.04	0.972	184.00
G (Binder to-aggregate ratio)	7.63	5.39	1.42	0.177	184.00
H (Curing age, day)	9.327	0.489	19.07	0.000	1.58
E ²	0.024	0.701	0.03	0.973	1.00
H ²	- 13.589	0.964	- 14.10	0.000	1.08
E × F	0.64	6.55	0.10	0.924	178.50
E × G	0.71	6.48	0.11	0.915	180.50
E × H	- 0.082	0.476	- 0.17	0.866	1.04
F × H	- 0.89	6.30	- 0.14	0.890	185.17
G × H	0.88	6.23	0.14	0.890	187.17

Table 8. Fitted (coded) coefficients for the compressive strength.

moderately correlated, and highly correlated if $VIF = 1, \geq 1 \leq 5$, and > 5 ^{6,8}. When VIF is higher than 10, there is significant multicollinearity. The degree of correlation for the independent variable (predictor), as shown in Table 6, revealed that binder ratio had a significant effect on slump, with VIFs yielding 1.00 and 1.50 for the linear and square models. Likewise, in Table 8, the binder ratio and curing age yielded significant effects on compressive strength, with VIFs exhibiting 1.54 and 1.58 for the linear model, 1.00 and 1.08 for the square model, and 1.04 for the 2-way interaction model. However, the degree of multicollinearity, as indicated in Tables 6 and 8, showed that water-to-binder ratio and binder-to-aggregate ratio have no significant effects on the slump and compressive strength. While multicollinearity does not reduce a model's overall predictive power, the effects

of water-to-binder ratio and binder-to-aggregate ratio on slump and compressive strength can be a subject for further investigative analysis. On the other hand, the curing age (H), as indicated in Table 7, demonstrated a significant effect on the compressive strength of blended cement concrete due to the P-value (0.00) that was lower than the significance level, while the F-value (363.62) was higher than 5.

The magnitude and significant effects of continuous variables on the slump and compressive strength of SNA-based cement concrete were determined by Pareto charts, and the results are shown in Fig. 6. From Fig. 6a, binder ratio crossed the reference line for the concrete slump, while curing age and its squared effect crossed the reference line for the compressive strength in Fig. 6a. These indicated binder ratio and curing age are statistically significant at the 0.05 significance level with the current model terms in influencing the workability and mechanical properties of blended cement concrete modified with SNA. Besides, these findings affirmed the results presented in Tables 5, 6, 7 and 8.

Following the model's ANOVA and fitted coefficients, the regression model between the response factor (slump, S) and the independent factors (E, F, and G) is illustrated in Eq. (7), while the relationship between the compressive strength (CS) and the continuous variables (E, F, G, and H) is displayed in Eq. (8). The model summaries yielded S, R²Adj, R² and Pred. R² of 1.63, 0.9905, 0.9619, and 0.7107 for the slump, and 1.72, 0.9846, 0.9732, and 0.9559 for the compressive strength. The Pred. R² of 0.7107 for slump suggests that the model may not generalize well to new data. The model performs better when S and R² are closer to 0 and 1³¹. Hence, the model relationships illustrated in Eqs. (7) and (8) can strongly forecast the responses (slump and compressive strength) of SNA-based blended cement concrete using binder ratio, water-to-binder ratio, binder-to-aggregate ratio, and curing age as the independent factors at 95% confidence and predictive intervals.

$$S \text{ (mm)} = 183 - 1755 E - 92 F - 242 G + 1000 E^2 + 1500 EF + 2500 EG \quad (7)$$

$$CS \text{ (MPa)} = 87 G + 1.02 H - 117 E - 4 F + 10 E^2 - 0.007890 H^2 + 127 EF + 235 EG - 0.039 EH - 0.21 FH + 0.35GH - 4 \quad (8)$$

Operating conditions

Operating conditions of independent variables on the slump

Figures 7, 8 and 9 display the visualized effects of the response surface of the slump based on continuous variables, such as binder, water-to-binder, and binder-to-aggregate ratios. The contour and 3D surface plots in Figs. 7, 8 and 9 demonstrated stationary ridge surfaces. Figure 7 shows that when the binder-to-aggregate ratio was kept constant at 0.23, there was less slump with an increasing binder ratio and a decreasing water-to-binder ratio. Similarly, Fig. 8 shows a reduced slump when the water-to-binder ratio is lowered, and the binder-to-aggregate ratio is raised while maintaining a constant binder ratio of 15 wt%. Figure 9 indicates a decreased slump with an increased binder ratio and increased binder-to-aggregate ratio when the water-to-binder ratio was maintained at a constant of 0.42. Nonetheless, any modification to the hold values changes the shape patterns of the independent factors⁶. As the color (green) gets lighter, the slump lessens. Concrete hydration can be attributed to the main cause of decreased slump with more binder content and a lower water-to-binder ratio. A stiffer mix with less slump results from a lower water-to-binder ratio because there is less water available to hydrate the cementitious particles. Furthermore, an increase in binder ratio without a commensurate rise in water exacerbates a stiffer mix³². The slump is further reduced because the cementitious particles absorb the water and initiate the hydration process more rapidly, speeding up the pace of stiffening. This makes the concrete mix less workable and more viscous³³. In general, concrete slump and workability are decreased by a binder's increased fineness and specific surface area (in this case, SNA in Table 1). This occurs because the mix becomes less fluid and more viscous due to the increasing surface area requiring more water for hydration reactions³⁴.

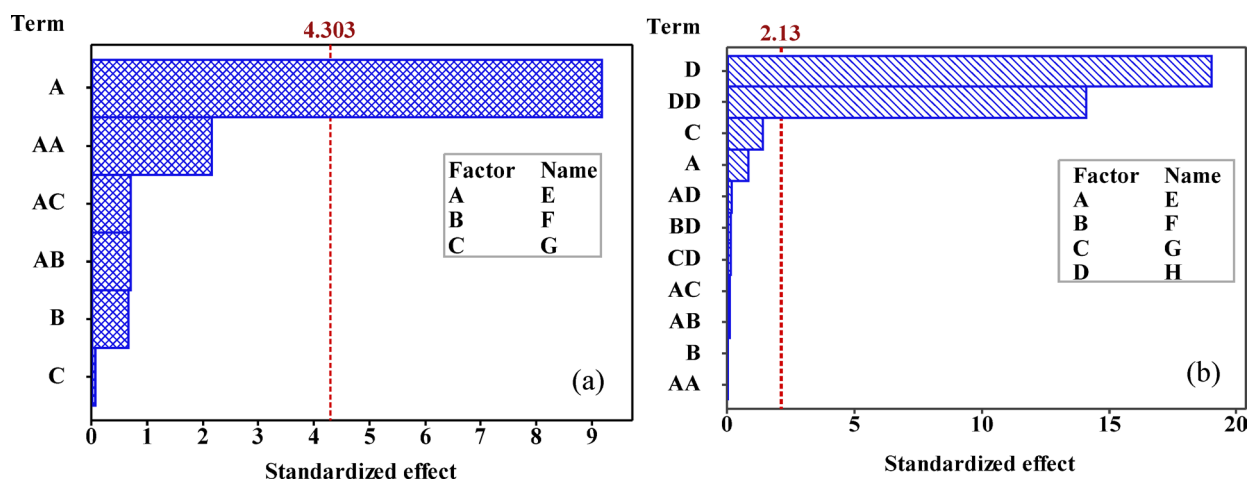


Fig. 6. Pareto charts of the standardized effects of continuous variables on (a) slump and (b) compressive strength.

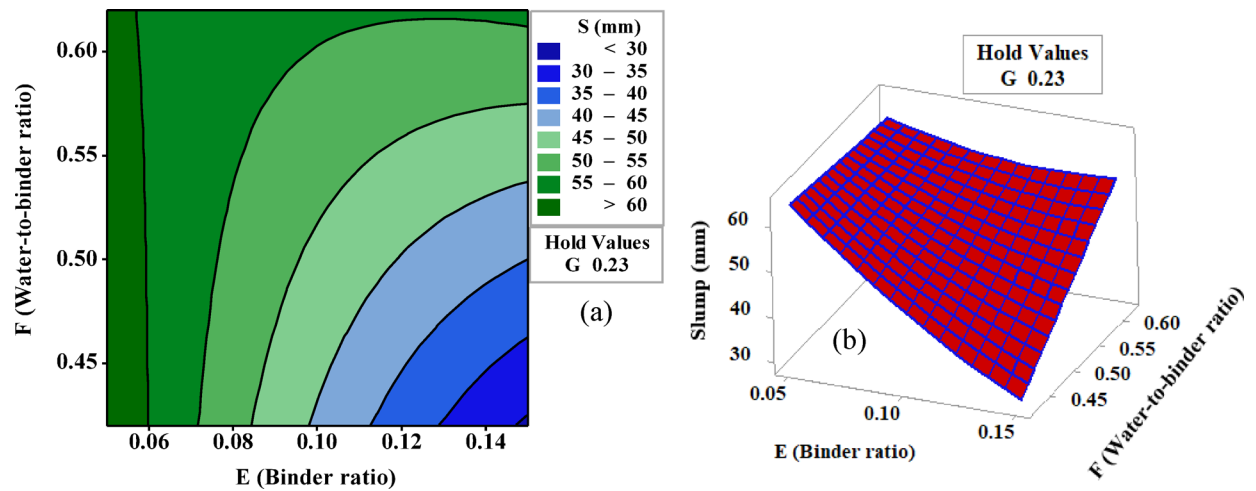


Fig. 7. Visualized effects showing (a) contour plot and (b) 3D surface plot of the slump response at 0.23 constant for binder-to-aggregate.

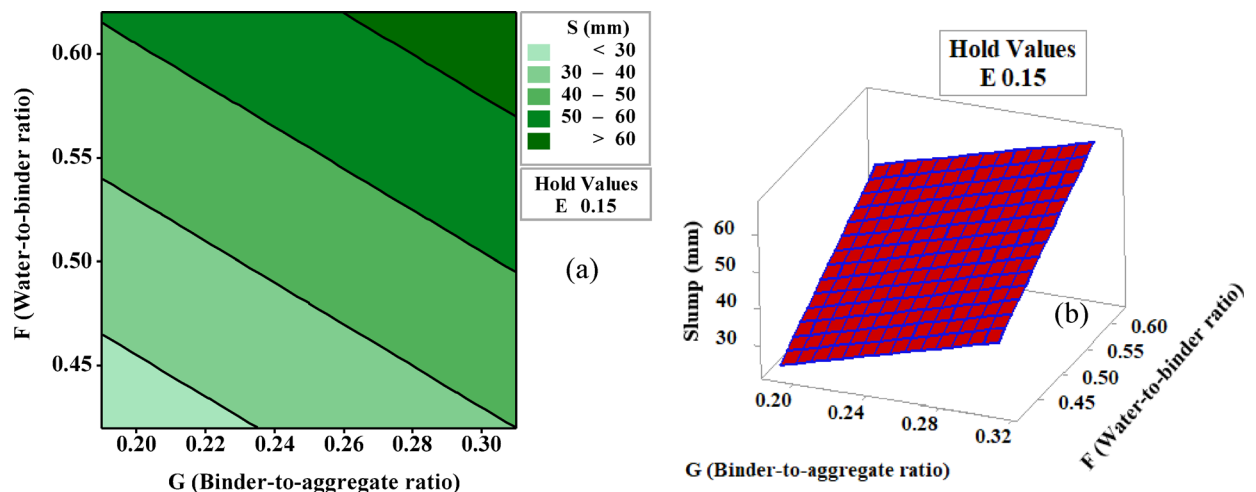


Fig. 8. Visualized effects showing (a) contour plot and (b) 3D surface plot of the slump response at a 0.15 constant for binder ratio.

A denser and more viscous paste is produced when there is a greater quantity of binder content in the mixture without an equal increase in water. This denser paste prevents the aggregates from flowing and moving freely, leading to less slump and firmer mix³⁵. A higher binder-to-aggregate ratio typically improves the slump of blended cement concrete, as the larger paste volume facilitates improved flow and compaction^{35,36}.

Operating conditions of independent variables on the compressive strength

Figures 10, 11, 12 and 13 illustrate the operating conditions of binder ratio, water-to-binder ratio, binder-to-aggregate ratio, and curing age on the compressive strength of blended cement concrete. As shown in Fig. 10, the compressive strength increased with increased binder-to-aggregate ratio and decreased water-to-binder ratio when binder ratio and curing age were maintained at constants of 15 wt% and 90 days. The highest compressive strength (> 50 MPa), as indicated in Fig. 10, occurred at binder-to-aggregate and water-to-binder ratios of 0.31 and 0.42. Figure 11 demonstrates increased compressive strength with increasing curing age and binder ratio, holding water-to-binder ratio and binder-to-aggregate ratio constant at 0.42 and 0.31. The highest compressive strength (> 55 MPa) in Fig. 12 was obtained at a 15 wt% binder ratio and 55–75 curing ages. Similarly, in Fig. 12, as the water-to-binder ratio decreased and the curing age increased, the compressive strength increased at constants of 0.10 and 0.23 for the binder and binder-to-aggregate ratios. Figure 13 shows that the compressive strength increased as the binder and binder-to-aggregate ratios increased, with constants of 0.42 and 90 for the water-to-binder ratio and curing age. Higher binder-to-aggregate and lower water-to-binder ratios in blended cement concrete typically create a denser and more compact concrete mix with fewer pores, resulting in higher compressive strength³⁵. A higher binder-to-aggregate ratio is demonstrated by more cementitious material to bind the aggregate particles. Consequently, the matrix gains density and cohesiveness, enhancing its compressive

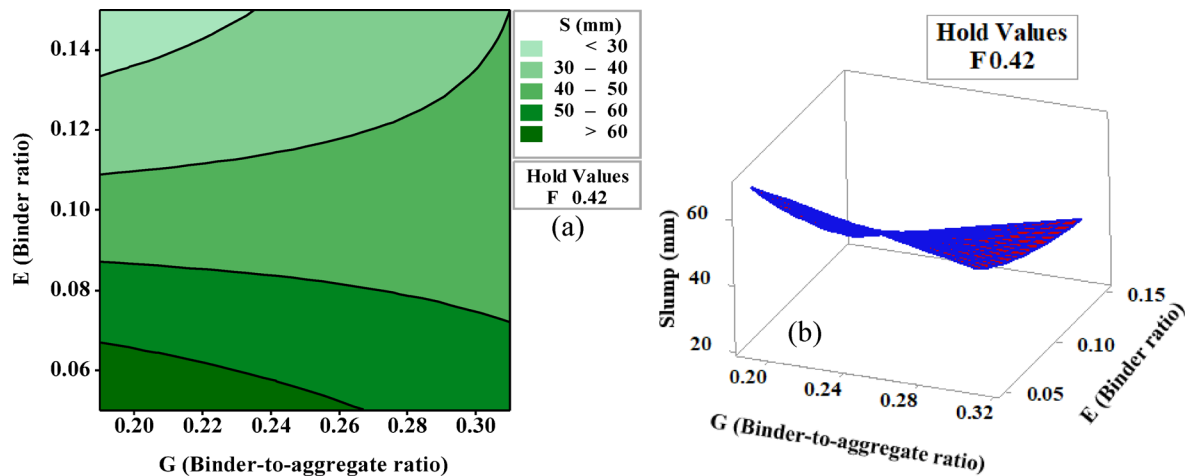


Fig. 9. Visualized effects showing (a) contour plot and (b) 3D surface plot of the slump response at a 0.42 constant for water-to-binder ratio.

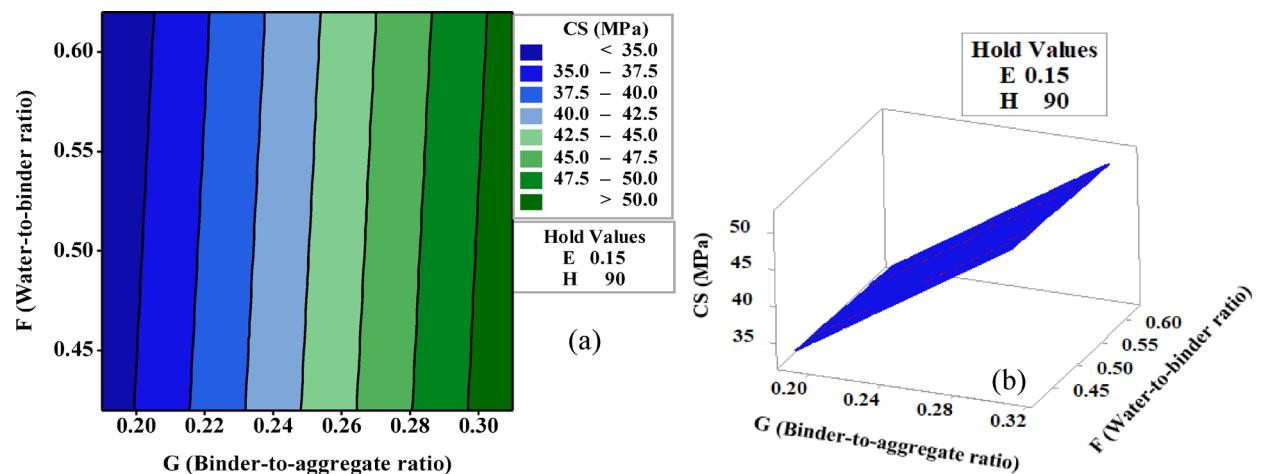


Fig. 10. Visualized effects showing (a) contour plot and (b) 3D surface plot of the compressive strength response at 0.15 and 90 constants for binder ratio and curing age.

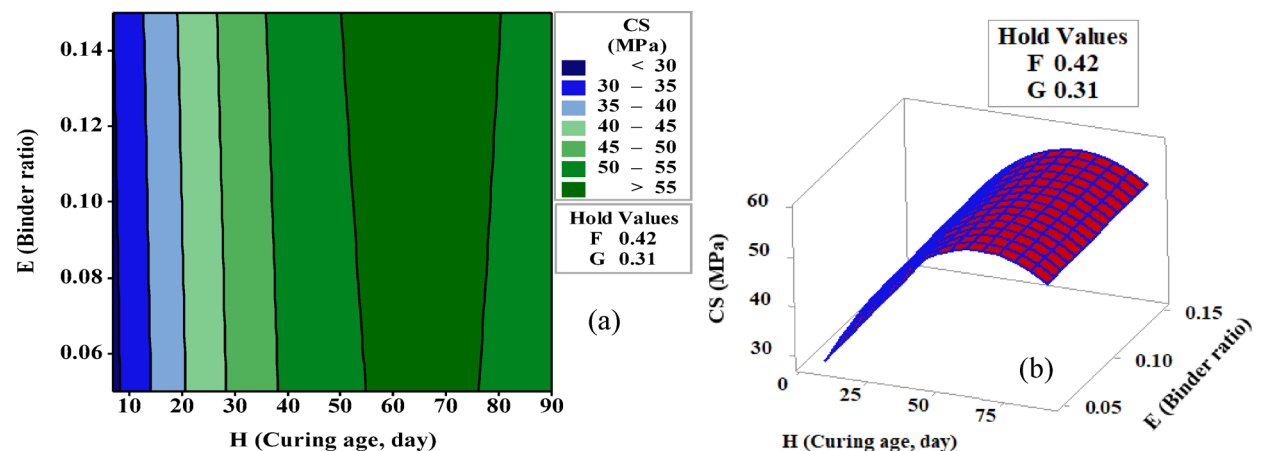


Fig. 11. Visualized effects showing (a) contour plot and (b) 3D surface plot of the compressive strength response at 0.42 and 0.31 constants for water-to-binder and binder-to-aggregate ratios.

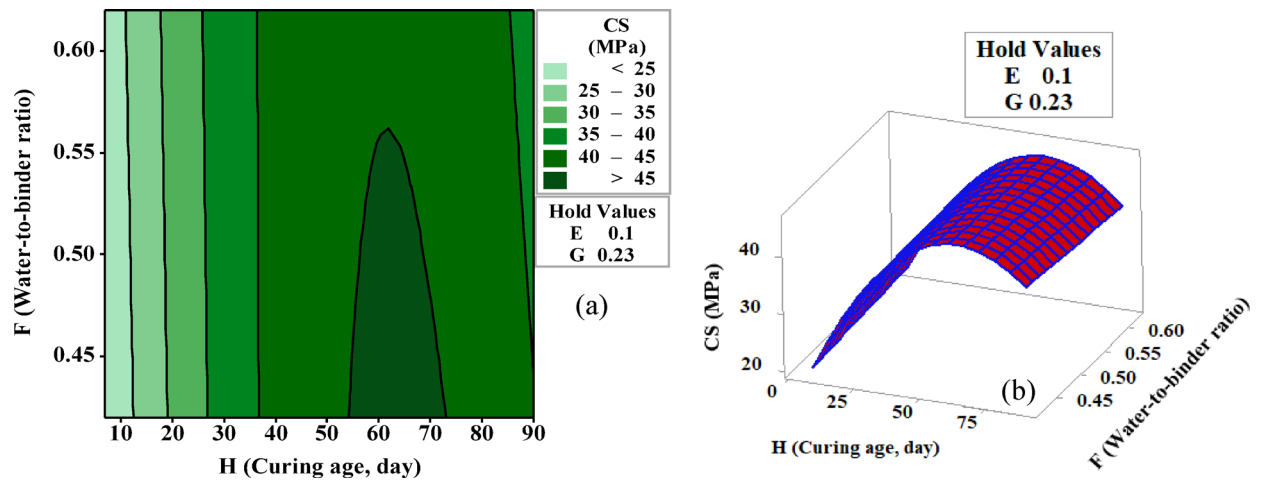


Fig. 12. Visualized effects showing (a) contour plot and (b) 3D surface plot of the compressive strength response at 0.10 and 0.23 constants for binder and binder-to-aggregate ratios.

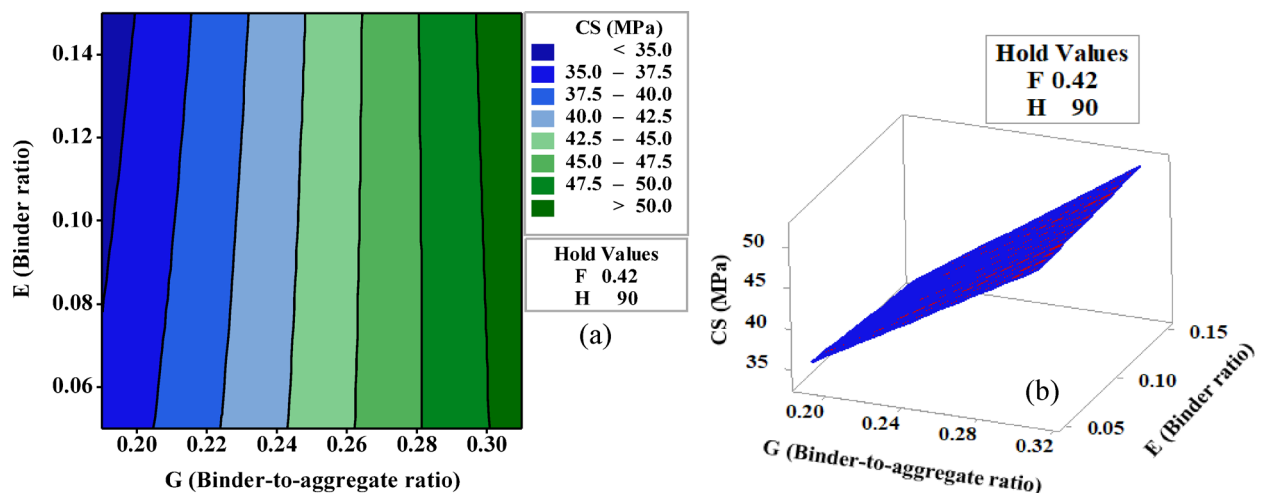


Fig. 13. Visualized effects showing (a) contour plot and (b) 3D surface plot of the compressive strength response at 0.42 and 90 constants for water-to-binder ratio curing age.

strength^{37,38}. A lower water-to-binder ratio signifies the presence of less water in the concrete mix, which is essential for the cement's hydration. The hydration process works more effectively with less water, resulting in the creation of a denser and stronger cement paste³⁹. Generally, the compressive strength of blended cement concrete rises with curing age, with the first 7–28 days yielding the most strength growth and subsequent strength development over longer ages³⁵. The BBD-RSM-based investigation on the properties of composite recycled aggregate concrete revealed that the replacement of cement with 5–15 wt% waste concrete powder and the water-to-binder ratio of 0.43 significantly enhanced the early-age and later-age of concrete¹⁴. Ultimately, the compressive strength of blended cement concrete is influenced by the binder ratio, water-to-binder ratio, binder-to-aggregate ratio, and curing age, serving as a guideline for the SNA utilization as a PLC substitute.

Optimization

Figure 14 displays the optimization values for the responses (slump and compressive strength) after combining the desirability functions into a composite desirability function (D). The Minitab 18 statistical program automatically presents a global answer, which is the optimal of all local solutions⁶. The universal solution combines the variable parameters to attain the required results on a 0–1 scale⁸. The current setting and current responses were indicated by the vertical and horizontal brown lines in Fig. 14a and b. The configuration in Fig. 14a optimized E (Binder ratio), F (Water-to-binder ratio), and G (Binder-to-aggregate ratio) as 0.150, 0.420, and 0.190, exhibiting a minimized slump of 24 mm at a D equals 1.000. These represent approximately a 40–63% decrease in a slump at a 95% confidence interval (CI) (–92.70, 140.70 mm) and 95% predictive interval (PI) (–92.90, 140.90 mm) compared to the slumps that yielded the highest and lowest compressive strengths. This result can be beneficial for self-supporting structures (lightly reinforced pavements or foundations) and compaction

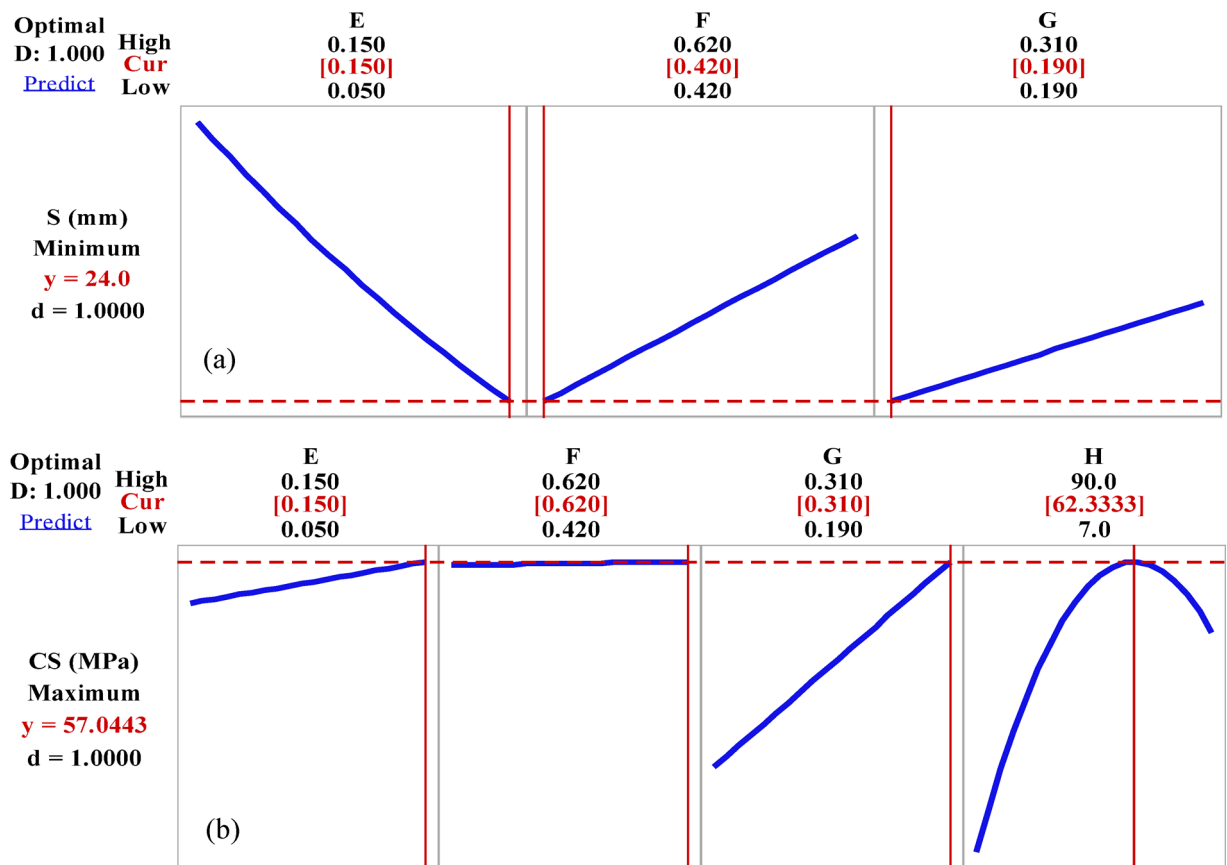


Fig. 14. Optimization of independent variables for (a) slump and (b) compressive strength.

ease. Nonetheless, it is crucial to take into account the particular project needs and any difficulties involved in its utilization. In the same vein, the current setting in Fig. 14b optimized E, F, G, and H as 0.150, 0.620, 0.310, and 62.33 curing age, demonstrating a maximized compressive strength of 57.04 MPa at 95% CI (17.90, 96.10 MPa) and 95% PI (17.80, 96.30 MPa) compared to the experimental compressive strength of 51.48 MPa. This indicates a roughly 10% rise in compressive strength.

Model validation

Figure 15 shows the correlation between the predicted response and the experimental findings using the fitted linear model regression equations shown in Eqs. (7) and (8). The results signified a strong correlation between the predicted response and experimental results. Figure 15a and b demonstrate that the models are 98.89 and 98.44% fit to optimize the slump and compressive strength at 95% CI and PI. In addition, the Pearson correlation coefficients (r) in Fig. 15a and b were larger than 0.80, indicating a strong correlation between the predicted and experimental values⁴⁰. These findings support a related study that optimized the strength of blended cement concrete modified with cashew nutshell ash, yielding a 99.92% R^2 fit to predict the relationship between the predicted and experimental compressive strengths³⁸.

Conclusions

This study recycles shea nutshell ash (SNA) and employs Box-Behnken design (BBD) to optimize the slump and compressive strength of blended cement concrete modified with SNA using C25, C30, and C40 MPa mix design proportions and tested for compressive strength after 7–90 curing ages. The response parameters (slump and compressive strength) were optimized by using binder ratio (E), water-to-binder ratio (F), binder-to-aggregate ratio (G), and curing age (H) as continuous factors. Comparisons and modeling were made between the predicted responses and the experimental values. The experimental and optimization findings led to the following deductions:

Binder ratio and curing age significantly influence the slump and compressive strength of blended cement concrete incorporating SNA compared to other continuous variables. The slump is optimized (minimized) at 15 wt%, 0.42, and 0.19 of binder, water-to-binder, and binder-to-aggregate ratios, exhibiting about 40–63% reduction compared to the experimental findings. The compressive strength is optimized (maximized) at 15 wt%, 0.62, 0.31, and 62.33 days of binder ratio, water-to-binder ratio, binder-to-aggregate ratio, and curing age, yielding approximately a 10% increment compared to the experiment results. The developed models exhibited

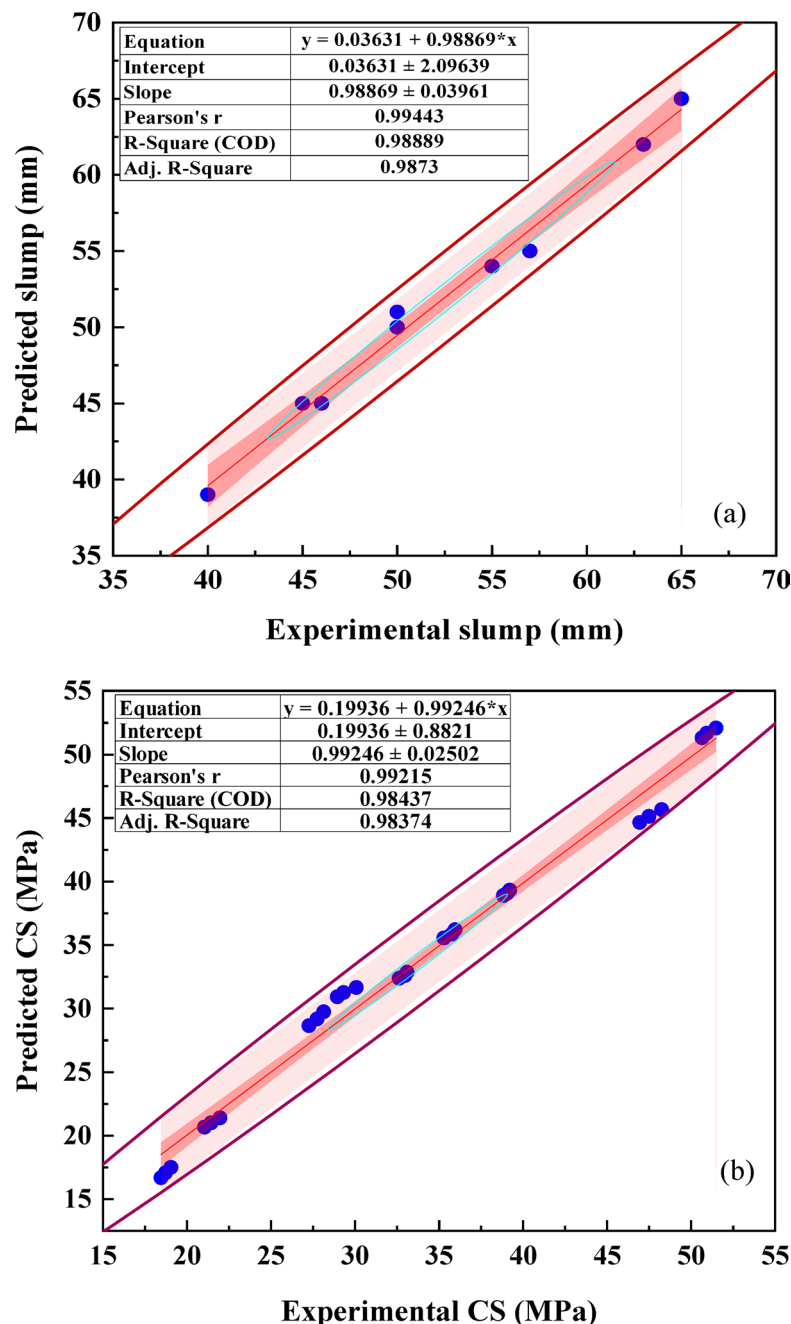


Fig. 15. Validation of developed models for (a) slump and (b) compressive strength.

strong correlations with 98.89 and 98.44% R^2 for validating predicted slump and compressive strength with experiment results.

This research establishes that BBD of RSM offers valuable behavioural models as an optimization method for blended cement concrete incorporating recycled agricultural waste, elucidating the relationship between responses and the continuous factors. The recycled material (in this case, SNA) has a higher specific surface area and fineness than PLC and meets 70% of the pozzolanic requirements for silica, alumina, and ferrite. These techniques facilitate concrete mix design, reduce testing requirements, simplify trial operations, and minimize material utilization. These are consistent with the building sector's dedication to sustainability.

Beyond the BBD as a response surface technique, it is important to explore additional techniques for further studies. These techniques include fractional factorial design, simplex centroid design, simplex lattice design, and central composite design.

Data availability

The datasets used and/or analyzed during the current study are available from the corresponding author upon reasonable request.

Received: 9 April 2025; Accepted: 23 June 2025

Published online: 12 July 2025

References

- Farooq, F. et al. Geopolymer concrete as a sustainable material: a state of the Art review. *Constr. Build. Mater.* **306**, 124762 (2021).
- Nandhini, K. & Karthikeyan, J. Sustainable and greener concrete production by utilizing waste eggshell powder as cementitious material—a review. *Constr. Build. Mater.* **335**, 127482 (2022).
- FAO. *World Food and Agriculture – Statistical Yearbook 2024* (FAO, 2024).
- Oyebisi, S. & Alomayri, T. Cement-based concrete modified with Vitellaria Paradoxa ash: a lifecycle assessment. *Construct. Build. Mater.* **342**, 127906 (2022).
- Zieve, P., Valley, P. P. K., Danso, H. & Antwi, K. Assessing the strength and durability behaviour of concrete enhanced with Kaolin clay and Shea nut shell particles. *Cogent Eng.* **11**, 2321384 (2024).
- Oyebisi, S., Owamah, H. & Ede, A. Flexural optimization of slag-based geopolymer concrete beams modified with corn cob Ash. *Scientia Iranica* **28** (5), 2582–2595 (2021).
- Onoue, K. & Bier, T. A. Optimization of alkali-activated mortar utilizing ground granulated blast-furnace slag and natural Pozzolan from Germany with the dynamic approach of the Taguchi method. *Constr. Build. Mater.* **144**, 357–372 (2017).
- Myers, R., Montgomery, D. & Anderson-Cook, C. *Response Surface Methodology: Process and Product Optimization Using Designed of Experiments* (John Wiley and Sons, Inc, 2009).
- Habibi, A., Ramezaniapour, A. M., Mahdikhani, M. & Bamshad, O. RSM-based evaluation of mechanical and durability properties of recycled aggregate concrete containing GGBFS and silica fume. *Constr. Build. Mater.* **270**, 121431 (2021).
- Habibi, A., Ramezaniapour, A. M. & Mahdikhani, M. RSM-based optimized mix design of recycled aggregate concrete containing supplementary cementitious materials based on waste generation and global warming potential. *Resour. Conserv. Recycl.* **167**, 105420 (2021).
- Wang, J. et al. Study on the optimum initial curing condition for fly ash and GGBS based geopolymer recycled aggregate concrete. *Constr. Build. Mater.* **247**, 118540 (2020).
- Montgomery, D. *Design and Analysis of Experiments* (John Wiley and Sons, Inc, 2005).
- Hurtado-Alonso, N., Manso-Morato, J., Revilla-Cuesta, V., Skaf, M. & Ortega-López, V. Optimization of cementitious mixes through response surface method: a systematic review. *Arch. Civil Mech. Eng.* **25**, 54 (2024).
- Li, H., Zhang, L., Liu, J., Chu, F. & Tian, Y. Study on the characteristics of composite recycled aggregate concrete based on Box–Behnken design response surface model. *Fractal Fract.* **7**, 648 (2023).
- Shao, W., Zha, W., Zhou, X. & Xu, T. Experimental study based on Box–Behnken design and response surface methodology for optimization proportioning of activated lithium slag composite cement-based cementitious materials. *Materials* **17**, 2651 (2024).
- Dai, C., Wu, A., Qi, Y. & Chen, Z. The optimization of mix proportions for cement paste backfill materials via Box–Behnken experimental method. *J. Institution Eng. (India): Ser. D.* **100**, 307–316 (2019).
- Aziz, A., Driouich, A., Felaous, K. & Bellil, A. Box–Behnken design based optimization and characterization of new eco-friendly building materials based on slag activated by diatomaceous earth. *Constr. Build. Mater.* **375**, 131027 (2023).
- Georgopoulos, G., Aspiotis, K., Badogiannis, E., Tsvilis, S. & Perraki, M. Influence of mineralogy and calcination temperature on the behavior of Palygorskite clay as a pozzolanic supplementary cementitious material. *Appl. Clay Sci.* **232**, 106797 (2023).
- BS EN 196-3. *Method Test. Cement: Phys. Test* (2016).
- BS EN 12620. *Aggregates from Natural Sources for Concrete*. (2013).
- BS EN 450-1. *Pozzolan for Use in Concrete: Definitions, Specifications, and Conformity Criteria*. (2012).
- BS EN 8615-2. *Specification for Pozzolan Materials for Use with Portland Cement: High Reactivity Natural Calcined Pozzolana*. (2019).
- BS EN 206. *Concrete Specifications, Performance, Production and Conformity*. (2016).
- BS EN 12390-2. *Testing Hardened Concrete: Making and Curing Specimens for Strength Tests*. (2019).
- BS EN 12350-2. *Testing Fresh Concrete Slump Test*. (2019).
- BS EN 12390-1. *Testing Hardened Concrete: Making and Curing for Strength Test*. (2019).
- Derringer, G. & Suich, R. Simultaneous optimization of several response variables. *J. Qual. Technol.* **12**, 214–219 (1980).
- Oyebisi, S. O., Ede, A. N. & Olutoge, F. A. Optimization of design parameters of Slag-Corncob Ash-Based geopolymer concrete by the central composite design of the response surface methodology. *Iran. J. Sci. Technol. - Trans. Civil Eng.* **45**, 27–42 (2021).
- Asadzadeh, S. & Khoshbayan, S. Multi-objective optimization of influential factors on production process of foamed concrete using Box–Behnken approach. *Constr. Build. Mater.* **170**, 101–110 (2018).
- Li, Z., Lu, D. & Gao, X. Multi-objective optimization of gap-graded cement paste blended with supplementary cementitious materials using response surface methodology. *Constr. Build. Mater.* **248**, 118552 (2020).
- Willmott, C. & Matsuura, K. Advantages of the mean absolute error (MAE) over the root mean square error (RMSE) in assessing average model performance. *Climate Res.* **30**, 79–82 (2005).
- Aitcin, P. C. Elsevier. The importance of the water–cement and water–binder ratios. in *Science and Technology of Concrete Admixtures* 3–13 (2016). <https://doi.org/10.1016/B978-0-08-100693-1.00001-1>
- Razeman, N. A. et al. A review on the compressive strength and workability of concrete with agricultural waste ash as cement replacement material. *IOP Conf. Series: Earth Environ. Sci.* **1135**, 012058 (2023).
- Zhang, M. et al. Effect of limestone powder fineness on the physical and mechanical performance of concrete. *Materials* **18**, 835 (2025).
- Neville, A. M. *Properties of Concrete* (Longman, 2011).
- Waqas, R. M., Butt, F., Zhu, X., Jiang, T. & Tufail, R. F. A comprehensive study on the factors affecting the workability and mechanical properties of ambient cured fly ash and slag based geopolymer concrete. *Appl. Sci.* **11**, 8722 (2021).
- Ahmad, A. et al. Prediction of compressive strength of fly ash based concrete using individual and ensemble algorithm. *Materials* **14**, 794 (2021).
- Oyebisi, S. et al. Optimising the workability and strength of concrete modified with anacardium occidentale nutshell ash. *Fibers* **9** (4), 1–16 (2021).
- Zhang, Q. et al. Hydration development of blended cement paste with granulated copper slag modified with CaO and Al₂O₃. *J. Mater. Res. Technol.* **18**, 909–920 (2022).
- Pei, Y. et al. Mix design optimization of high-viscosity asphalt mixtures for ultra-thin pavement considering geometric properties and interface slip behavior for aggregate system. *Constr. Build. Mater.* **464**, 140085 (2025).

Acknowledgements

The authors are thankful to the Research Support Directorate of Durban University of Technology, Durban, South Africa, for supporting this work.

Author contributions

S.O. conceptualized and designed the study, collected the data, analyzed and interpreted the results, S.O., M.I.S., S.M., and B.P.K. analyzed the data with software, and wrote and reviewed the manuscript. All authors have read and agreed to the published version of the manuscript.

Funding

The authors declare that no funds, grants, or other support were received during the preparation of this manuscript.

Declarations

Competing interests

The authors declare no competing interests.

Consent to publish

Not applicable.

Additional information

Supplementary Information The online version contains supplementary material available at <https://doi.org/10.1038/s41598-025-08745-1>.

Correspondence and requests for materials should be addressed to S.O.

Reprints and permissions information is available at www.nature.com/reprints.

Publisher's note Springer Nature remains neutral with regard to jurisdictional claims in published maps and institutional affiliations.

Open Access This article is licensed under a Creative Commons Attribution-NonCommercial-NoDerivatives 4.0 International License, which permits any non-commercial use, sharing, distribution and reproduction in any medium or format, as long as you give appropriate credit to the original author(s) and the source, provide a link to the Creative Commons licence, and indicate if you modified the licensed material. You do not have permission under this licence to share adapted material derived from this article or parts of it. The images or other third party material in this article are included in the article's Creative Commons licence, unless indicated otherwise in a credit line to the material. If material is not included in the article's Creative Commons licence and your intended use is not permitted by statutory regulation or exceeds the permitted use, you will need to obtain permission directly from the copyright holder. To view a copy of this licence, visit <http://creativecommons.org/licenses/by-nc-nd/4.0/>.

© The Author(s) 2025